J Fail. Anal. and Preven.
https://doi.org/10.1007/s11668-022-01413-w

LESSONS LEARNED

Heat Transfer, Thermal Stress and Failure Inspection of a Gas Turbine Compressor Stator Blade Made of Five Different Conventional Superalloys and Ultra-High-Temperature Ceramic Material: A Direct Numerical Investigation

Abyaz Abid · Md Tanbir Sarowar

Submitted: 4 April 2022 / in revised form: 7 May 2022 / Accepted: 9 May 2022

Abstract Probing the efficiency of Brayton cycle is of great importance to harbor maximum output from gas turbines. The efficiency of Brayton cycle largely depends on the maximum temperature of the cycle. However, maintaining a very high temperature in a gas turbine is restricted due to various metallurgical problems developed within the compressor blade surface, which result in the structural failure of gas turbine compressor. To address these problems, numerous prospective solutions are proposed among which materials' selection and preference for specific parts of a gas turbine are highly celebrated among researchers. Although many works are dedicated especially to the rotor blades of the turbine compressor, the stator blades which are integral component of the turbine compressor as they partially convert high velocity into high pressure to increase the pressure from the preceding stage and have both functional criteria and failure mechanism unlike the rotor blades—are yet to receive enough attention in terms of material research and development. On the other hand, recent advancements in the refractory properties of ultra-high-temperature ceramics make them highly potent materials to incorporate in the gas turbine and manufacturing industry. The proposed article seeks to explore this scope of material research specifically for the stator blades of gas turbine compressors through a numerically performed performance analysis. To provide better insight about future reach of the scope, the performance analysis is conducted among four different superalloys which are already established as rotor blade materials—Inconel 718, Ti–6Al–4V, Nimonic 80A, GTD 111 DS and an ultra-high temperature ceramic material—NbB_2 as potential stator blade material in terms of thermal distribution, thermal stress and displacement over the blade surface. Reports showed that—NbB_2 undergoes the least thermal displacement, whereas Ti–6Al–4V exhibits the least thermal stress during the operational stage. Considering the overall performance—Inconel 718 and Nimonic 80A failed as potential stator blade materials, whereas NbB_2 and GTD 111 DS can only withstand the extreme condition inside the compressor with safety factor of one. The article concludes with Ti–6Al–4V as the most potent stator blade material to be incorporated into the gas turbine industry.

Keywords Gas turbine · Failure analysis · Thermal stress · Niobium diboride · Numerical method

List of Symbols

T_{ext}	Temperature of the external fluid
q_0	Heat flux (W/m^2)
h	Convective heat transfer coefficient (W/m^2 K)
D	Elasticity tensor
C	Heat capacity (J/kg K)
k	Thermal conductivity (W/mK)
S_{ut}	Ultimate tensile strength
S_{uc}	Ultimate compressive strength
E	Young's modulus
u	Displacement vector
n	Factor of safety
Ti–6Al–4V	Grade 5 titanium (UNS R56400)
NbB_2	Niobium diboride
GTD 111 DS	Directionally solidified superalloy
CTE	Coefficient of thermal expansion
k_s	Stiffness of spring

A. Abid (✉) · M. T. Sarowar
Department of Mechanical and Production Engineering, Islamic University of Technology (IUT), Board Bazar, Gazipur 1704, Bangladesh
e-mail: abyazabid@iut-dhaka.edu

Published online: 24 May 2022

Pr	Prandtl number
Re	Reynolds number
Nu	Nusselt number
H	Characteristic length of cooling air
x	The distance from the beginning of the blade (in meter)
R_p	Compression ratio
C_p	Heat capacity at constant pressure
C_v	Heat capacity at constant volume

Greek Letters

ρ	Density (kg/m^3)
σ	Thermal stress
ε	Thermal strain
α	Coefficient of thermal expansion
σ_v	Von Mises stress
σ_x, σ_y, σ_z	Normal stresses along x, y and z directions, respectively
τ_x, τ_y, τ_z	Shear stresses along x, y and z directions, respectively
σ_A	Principle stress (tensile)
σ_B	Principle stress (compressive)
υ	Poisson ratio
$\varepsilon_x, \varepsilon_y, \varepsilon_z$	Thermal strain along x, y and z directions, respectively
τ_{ij}	Shear stress tensor
ε_{ij}	Strain tensor
∇	Vector differential operator
μ	Dynamic viscosity (Pa s)
γ	Ratio of heat capacity at constant pressure to constant volume
η	Thermal efficiency

Subscripts

ut	Ultimate tensile strength
uc	Ultimate compressive strength
x, y, z	x, y, z direction
s	Spring
i, j	Two-dimensional tensor
p	Constant pressure
v	Constant volume

Introduction

With the increase in the global population, power consumption in various energy and technology sectors is more on the rise than ever. The average annual consumption growth rate is expected to be tripled within the next 60 years [1, 2]. In this prospect, industrial and energy consummate technologies will play crucial roles in meeting the subsequent energy needs of the next-generation world. Even though renewable energy resources have shown great promise through various appliances and received good responses through constant research outputs [3–6], gas and steam turbines are still required to accomplish the ultimate mass-energy demand. Basic principle and working procedure of gas turbines have been provided in previous works of various authors with necessary simplifications and assumptions [7–10]. Gas at room temperature and pressure is introduced through the inlet of the compressor and compressed with high temperature and pressure. Highly compressed gas with higher temperature then enters the combustion chamber to produce work in the gas turbine cycle. The temperature change in the compressor causes a great degree of temperature variance, and as a result, the rotor blades of the first-stage compressor experiences a very-high-temperature gradient. According to the basic functions of gas turbine powerplant [7], the net power and thermal efficiency of gas turbine depend on two important parameters—pressure ratio and temperature of inlet air. Higher pressure ratio in gas turbine compressor will result in higher efficiency and net work done by the gas turbine cycle [8]. The related equation is:

$$\eta = 1 - R_P^{\frac{(1-\gamma)}{\gamma}} \quad \text{(Eq 1)}$$

where η is the efficiency of Brayton cycle, R_P is the compression ratio of the Brayton cycle and $\gamma = \frac{C_\mathrm{P}}{C_\mathrm{V}}$ is the ratio of specific heat capacity at constant pressure to specific heat at constant volume. Higher compression ratio is the effect of higher displacement volume of gas, which is due to the higher temperature in the compressor. Although higher temperature of the compressed gas will increase the efficiency of the gas turbine cycle, there are numerous metallurgical problems that are associated with the stator blade's continuous exposure to hot temperature [11, 12]. Park and Choi investigated the impact of the Strouhal number on the convective heat transfer coefficient (CHTC), which is responsible for the transition of unsteady state to steady-state heat transfer. This phenomenon results in the uneven temperature distribution within the blade and raises the thermal gradient along the blade surface [13]. Under continuous increase in thermal stress due to operating at hot temperature and being one of the most sensitive parts of the gas turbine, the stator blade develops significant thermal stress that can lead to the plastic deformation and total rupture of the turbine compressor [14, 15].

A series of mechanical analysis for the gas turbine stator blade has been covered in [12] with an estimation that the maximum thermal stress developed in the trailing corners of the gas turbine. Qu et al. [14] presented two different expositions to the failure of gas turbine because of concentrated thermal stress in the trailing edges. One of those reasons is fatigue failure, and the other is the origination of instant cracking in the leading and trailing edges. Due to

the fatigue failure and propagation of crack formation in the blade in high-temperature condition, proper study and accurate anticipation of the heat transfer parameters of the stator blade are very important to reduce the maintenance and repair cost [15]. Various active and passive methods for cooling the turbine blade have been in consideration lately. However, most of these processes incorporate thermal cooling of the blades, which result in substantial decrease in the efficiency of gas turbine [16–18]. On the other hand, incorporating different super alloys and ceramic materials in gas turbine blades that can withstand high-temperature conditions without showing any declination in the efficiency of the turbine holds much more promise. Different types of alloys, such as nickel-based, titanium-based, cobalt-based and aluminum-based alloys, have been proposed as the prospective materials to use in turbine blades [19].

Nickel–titanium-based alloys had been used in earlier works of different authors and have lately been proven materials with good compressive strength for industrial applications [18, 20, 21]. Inconel 718 has already been proposed as a gas turbine blade material and has been recognized as one the most successful superalloy ever used in gas, steam, and air jet engines due to its amazing qualities suitable for propulsion industries—balance of properties, reasonable cost, capability and forgeability. This superalloy has been largely used in machining and drilling applications as well as in aircraft and aerospace industries for its high creep resistance [22, 23]. A study had been conducted by A. Thomas et al. and E. Hosseini regarding the development of mechanical properties, aging characteristics, thermal deformation mechanism at temperature as high as 1200 K in [24, 25]. Development of additively manufactured Inconel 718 has shown higher tensile strength post-high-temperature treatment compared to other wrought alloys and materials, which has opened the door for future possibility of applying the alloy in hot temperature conditions with relatively low metallurgical problems [26]. Failure analysis of a gas turbine rotor blade made of Inconel 718 has been investigated, which analyzed the first-stage compressor rotor blades of gas turbine that are subjected to high-cycle fatigue mechanism (HCF) [27]. Probable reason for this failure is estimated as the origination of fatigue cracks near the leading edges of rotor blades because of the constant tensile stress developed in the blades due to centrifugal force. However, a numerical approach to determine the failure criterions of a stator blade made of Inconel 718 is yet to be investigated where the developed stress is a thermal stress that is compressive in nature.

Possessing high weight-to-strength ratio, corrosion resistance, high application temperature, titanium alloys has been recognized as one of the most widely used materials in modern world heavy industries [28, 29]. Since the inception of titanium alloys, Ti–6Al–4V has been in the discussion because of its various flexibility and high machinability features. Experimental study along with numerical analysis inspected failure analysis of a turbine blade made of Ti–6Al–4V [30]. Due to the centrifugal force associated with high-speed rotation of the turbine blade, tensile stress develops in the blade root region. SEM investigation in the study showed that different aspects of fretting fatigue initiate multiple cracks and high surface roughness at the contact edges—which ultimately results in the failure of the turbine blade. An innovative approach of incorporating titanium alloys in gas turbine application has been conducted in [31]. Results showed an analysis of inside deformation and temperature uniformity within the forged Ti–6Al–4V blade with respect to certain parameters—initial workpiece temperature, smaller friction factor and shorter dwell time. Despite various prospects about using Ti–6Al–4V titanium alloy in turbine blades proposed in many scientific works, numerical analysis showing the failure criteria for a turbine stator blade of Ti–6Al–4V is yet to accomplish in order to solidify the use of Ti–6Al–4V as stator blade material for gas turbine.

GTD 111 DS is a nickel-based alloy, which was used primarily as the blade material since the inception of gas and air jet turbine [32]. Sabri et al. [33] studied the pitting corrosion and oxidation phenomena inside the turbine blade made of GTD 111 DS alloy. The work sincerely investigated the plastic deformation and wear debris that are initiated within the first stage of the turbine blade due to excessive overheating caused by constant high rate of heat exchange by the flow of hot gas and the presence of erosion cavities. Visual and microstructural testing was conducted upon two stages GTD 111 DS blade of gas turbine in [34]. Results showed that even after 24000 h of exposure of the turbine blades to the high-speed flow of hot gas, the base material showed no cracks, and neither degraded microstructure of GTD 111 DS alloy was observed.

Ultra-high-temperature ceramics have been evolved as one of the prime contenders to use as a base material in gas turbine rotor blades in recent times. Because of their chemical, metallurgical and physical stabilities at high temperature and pressure, high yielding strength and melting point have been in consideration as a proper material for different components of gas turbine [8]. Several experimental analyses showed that UTHC (ultra-high temperature ceramics) such as borides, nitrides and carbides has shown high resistivity [35], high melting points [36] and high thermal coefficient [37–39] in extreme temperature. A similar numerical approach has been taken in [40] to show the probability of using HfB_2 as a potential stator blade material. The output envisioned that the material could withstand the compressive stress with a

safety factor of 1.28 K. Vaferi et al. incorporate ZrB_2 and TiB_2 for the similar prototype, and it has been validated that both of these materials show higher-temperature distribution uniformity compared to ZrB_2 and consequently impart less thermal stress on the stator blade [41, 8]. Changes in the stability and other mechanical properties of the respective materials have been brought by developing SiC-reinforced composites made of HfB_2, ZrB_2 and TiB_2 [42–44]. Finite element analysis has been executed for the composite materials in order to assess the thermal stress, temperature distribution and resultant displacement developed in the material [45]. Numerical results show that ZrB_2–SiC provides better thermal conductivity and lower thermal expansion compared to HfB_2–SiC. Due to lower thermal gradient along the surface of the ZrB_2–SiC stator blade developed much less thermal stress compared to HfB_2, NbB_2 is one of the most potential borides—showing similar characteristics to ZrB_2, HfB_2 and TiB_2 such as its higher hardness [46], smooth surface morphology [47], higher resistance at elevated temperature, higher wear resistance and higher fracture toughness [48]. However, NbB_2 is yet to be embodied in turbine industry like its neighboring borides and so this paper investigates the possible inclusion of this ceramic as a gas turbine stator blade material.

Nickel-, chromium-, titanium- and aluminum-based superalloy—Nimonic 80A—is widely used in the field of industrial application. Better wear resistance, high hardness and relatively high toughness, adequate thermal shock properties and excellent chemical stability and machinability have been proved for Nimonic 80A [49–51]. Due to their functional ability at higher temperature, Nimonic 80A has been experimented earlier as a base material for different components in the field of aerospace, turbomachinery, propulsion industry, marine engineering, automobile and so on [52, 53] A static structural model analysis of a gas turbine rotor blade made of Inconel 625, Nimonic 80A and Super alloy X has been conducted in terms of selection of blade profile, material and vibration in [54]. The most equipped one as a potential rotor blade material is judged upon three different revolution speeds (RPM) at 20,000, 40,000 and 60,000 showing Nimonic 80A imparting maximum stress for all the three cases. A comprehensive computational approach for different Nimonic materials has been proposed by Khawaja et al. with defined operating conditions within turbine and a safety factor of 1.33 by a nonlinear Multiphysics finite element analysis [55]. R. Subbarao and N. Mahato compared four different Nimonic materials, which incorporated Nimonic 105, 90, 80 and 263 both numerically and experimentally, and concluded that Nimonic 80A has a moderate outcome of thermal stress, distribution and displacement over other materials [56].

A sincere walkthrough over most of the recent and previous works of different researchers explores that a good amount of those works concentrates mostly on the thermal stress and failure analysis of first-stage compressor rotor blades of gas turbine. However, the first-stage compressor stator blades are yet to have sufficient attention and convincing outcome compared to its counterpart rotor blades. Main motivation of the current study is to investigate the strength of the first-stage compressor stator blades under extreme thermal conditions in terms of thermal stress and resultant displacement. The extensive literature review of this paper exhibits that the working materials—Inconel 718, Ti–6Al–4V, Nimonic 80A and GTD 111 DS had been around the turbine and propulsion industry since the inception of mainstream research on the gas turbine components. High corrosion resistance, high transformation temperature range, good wear resistance, excellent hardness under high thermal condition and impressive ultimate yield strength make these alloys highly potent to incorporate in the turbine stator blade material industry [57]. Recent advancements of the research and development field of ultra-high-temperature ceramics envision potential application of UTHC such as NbB_2 as gas turbine stator blade material mentioned previously. Approach carried out in [40, 41, 8] taking ZrB_2, TiB_2 and HfB_2 as the potential stator blade materials is similar to this paper reveals great promise for ultra-high-temperature ceramic-based gas turbine stator blades.

The presenting paper follows heat transfer and thermal stress analysis of the turbine stator blades made of the studied materials—Inconel 718, Ti–6Al–4V, Nimonic 80A, NbB_2 and GTD 111 DS alloy to inspect their true potentials as stator blade material. A three-dimensional model of first-stage compressor stator blade of gas turbine has been considered for the simulation work along with necessary physics and boundary conditions. Upon validation of the work, five different materials are taken into consideration to compare their performances in extreme thermal conditions. Three different grids are applied to the 3D geometry of the stator blade to obtain mesh independence. Thermal stress, temperature distribution and resultant displacement of each individual stator blade materials are calculated numerically for optimum number of elements found from the applied grid test of the static structure of the stator blade, and the results are showed in corresponding figures. Lastly, based on those results a comparative study has been done with respect to the factor of safety for each of the five materials to find out the most competing material to incorporate in gas turbine stator blade industry.

Methodology

Geometry

The stator blade model and its different parts are shown in Figs. 1 and 2. Due to constant exposure to high temperature during operation, the stator blade is vulnerable to different types of metallurgical problems, such as oxidation, corrosion and sulfidation. For preventing this type of problems, cooling blade is mounted in stator blade, as introduced in Fig. 3. The duct within the cooling blade is used to flow the cooling air at pressure of 30 bar and temperature of 600 K through the stator blade to cool it by heat convection. Since the work concentrates mostly on the materials applied on the blade, the relative complexities that come with geometrical details of the ribs inside the cooling ducts have been ignored [58].

Governing Equations

The corresponding work includes two important sets of governing equations: 1. heat diffusion equation for showing the thermal behavior of the stator blade model and 2. the linear elastic equations that match the impacts in the mechanical properties due to ceaseless heating. The first-stage compressor stator blades of gas turbine are exposed to the flow of highly compressed hot gas. As a result, the temperature of the stator blades remains quite high during the operation of turbine. The heat is dissipated from the combustion gases to the stator blade by convection and conduction. The convection heating process maintains Newton's law of cooling from

$$q_0 = h(T_{\text{ext}} - T) \quad \text{(Eq 2)}$$

here q_0, h, T_{ext}, T represent the heat flux, convective heat transfer coefficient, temperature of the external fluid and temperature of the solid surface, respectively. In this study, solid surface is simply the surface of the stator blade and external fluid is the highly compressed gas that meets it.

The heat dissipation through conduction from the stator blade surface follows the equation of heat [8]

$$\rho C \frac{\partial T}{\partial t} = \nabla.(k \nabla T) \quad \text{(Eq 3)}$$

where ρ, C, k, T are defined to density, heat capacity, thermal conductivity and temperature, respectively. ∇ (Nabla) is called the vector differential operator, which is applied for the function in one-dimensional domain

$$\nabla T = \frac{\partial T}{\partial x} + \frac{\partial T}{\partial y} + \frac{\partial T}{\partial z} \quad \text{(Eq 4)}$$

Equation 4 represents the temperature gradient with respect to the position of the blade along x, y and z axes.

It is to be noted that due to temperature gradient the temperature distribution over the stator blade will not be congruous. Also, the fact that stator blade is fixed in both sides will cause thermal stress for the stator. This thermal stress along three dimensions can be identified by the corresponding linear elastic equation. For the current work, Duhamel–Hook equation is considered for finding the thermal stress developed along the stator blade material [41]. The law is as follows

$$\sigma = D(\varepsilon - \alpha(T - T_{\text{ref}})) \quad \text{(Eq 5)}$$

here σ is the thermal stress, ε is the strain, D is the elasticity tensor, α is the coefficient of thermal expansion, T is the temperature at which thermal stress is to be calculated. Also, the reference temperature, T_{ref} is taken to be 300 K. Initial stress and strain are not taken into consideration.

The material is taken to be isotropic, and due to this, D—the stiffness matrix of the material is symmetric. It has a 3 × 3 matrix indicating the three components of thermal stress [45]

$$\begin{bmatrix} \sigma_x \\ \sigma_y \\ \sigma_z \end{bmatrix} = \frac{E}{(1+\upsilon)(1-2\upsilon)} \begin{bmatrix} 1-\upsilon & \upsilon & \upsilon \\ \upsilon & 1-\upsilon & \upsilon \\ \upsilon & \upsilon & 1-\upsilon \end{bmatrix} \begin{bmatrix} \varepsilon_x \\ \varepsilon_y \\ \varepsilon_z \end{bmatrix} \quad \text{(Eq 6)}$$

where σ, ε, υ are the stress, strain, and Poisson's ratio, respectively. E is the Young's modulus. Also, the stain tensor for solid domain can be defined as [8]

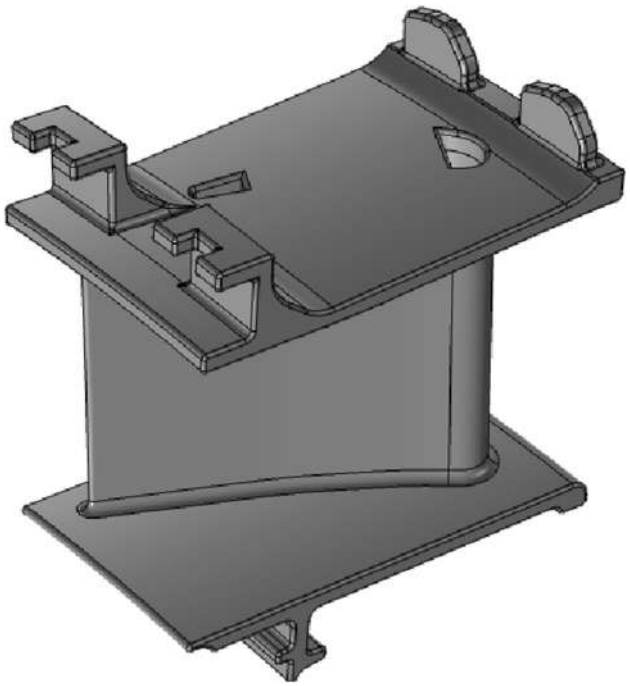

Fig. 1 Three-dimensional isometric view of a gas turbine stator blade

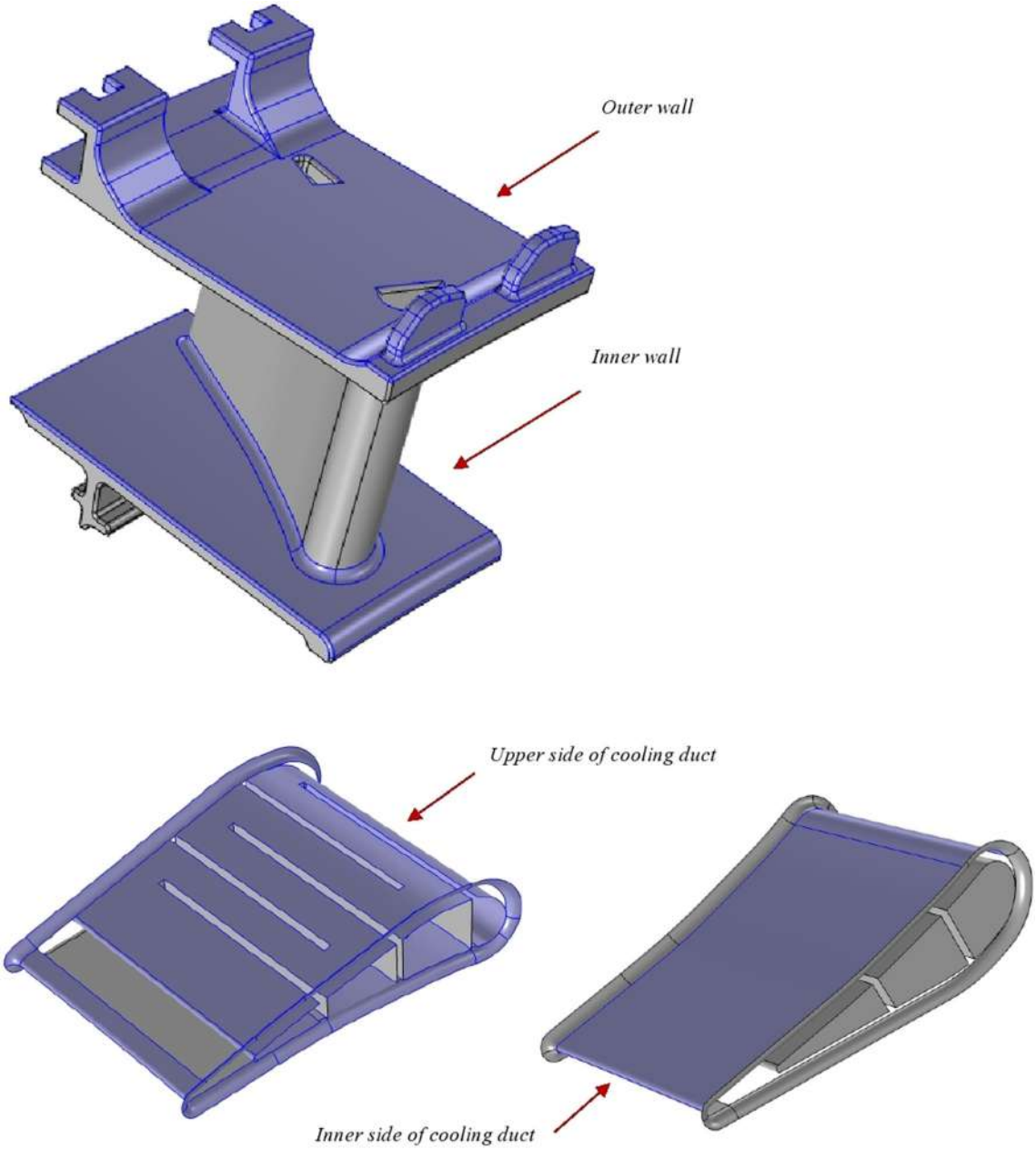

Fig. 2 Different parts of 3D static model of gas turbine stator blade

$$\varepsilon = \frac{\nabla\vec{u} + \nabla\vec{u}^{T}}{2} \quad \text{(Eq 7)}$$

where $\boldsymbol{u}$ shows the displacement vector. The relationship between the strain and shear component for the two-dimensional system is a function of Young's modulus and Poisson's ratio [41]

$$\tau_{ij} = \frac{E\varepsilon_{ij}}{(1-2\upsilon)} \quad \text{(Eq 8)}$$

The deformation rate of the stator blade material due to the constant exposure to hot temperature is dependent upon three factors—material properties, applied load and exposed temperature [8]. Among the proposed materials for the study, most of them are ductile materials that show high plasticity and malleability without fracture when huge amount of stress is impinged upon. Depending on the thermal conductivity and coefficient of thermal expansion of the materials, the stator blade conducts heat along its surface and due to the fixed supports at the ends it deforms as there is little chance of free expansion. In this case, the thermal stress is evident in tensile nature.

The equations for von mises theory which estimates the possibility of failure by measuring both the compressive

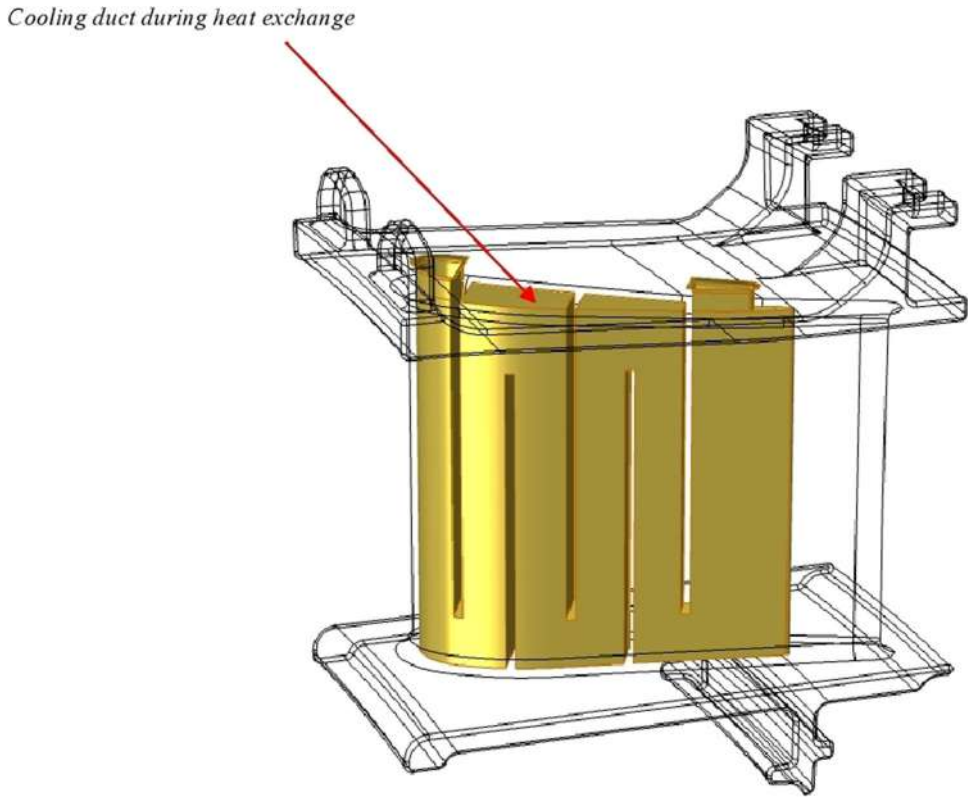

Fig. 3 Wireframe rendered view of internal cooling duct of first-stage compressor stator blade of gas turbine

and tensile strength of the materials are presented in Eq 9 along with Eqs 10 and 12. The equations are as follows [8]:

$$\sigma_v = \sqrt{\frac{(\sigma_x - \sigma_{y)}^2 + (\sigma_z - \sigma_y)^2 + (\sigma_x - \sigma_z)^2 + 6\left(\tau_{xy}^2 + \tau_{xz}^2 + \tau_{zy}^2\right)}{2}} \quad \text{(Eq 9)}$$

$$\sigma_A = \frac{S_{\text{ut}}}{n} \quad \text{(Eq 10)}$$

$$\frac{\sigma_A}{S_{\text{ut}}} - \frac{\sigma_B}{S_{\text{uc}}} = \frac{1}{n} \quad \text{(Eq 11)}$$

$$\sigma_B = -\frac{S_{\text{uc}}}{n} \quad \text{(Eq 12)}$$

here σ_v, σ_x, σ_y, σ_z represent von Mises stress and normal stresses along x, y, z directions. Similarly, τ_x, τ_y, τ_z are denoted for shear stresses along x, y, z directions. σ_A, σ_B are for principal stresses. S_{ut} is the ultimate tensile strength and S_{uc} is the ultimate compressive or the yield strength. To be noted that n is taken here as the factor of safety for failure analysis of the turbine blade. As existence of thermal gradient and its subsequent thermal stress cause the tensile strength of alloys to be dominant, the von mises criteria of failure are more convenient for the failure analysis of stator blades of gas turbine.

Material Properties

Prospected nickel- and titanium-based superalloys are the prime contenders as suitable gas turbine blade materials due to their ability to withstand elevated temperature by forming thick, stable passivating oxide layer, which protects the blade from further attack. They have high oxidation resistance up to 1600 °C along with exceptional high temperature resistance, low density, fracture toughness, impact resistance and improved environmental resistance [59]. Likewise—the ultra-high-temperature ceramics such as NbB_2 have recently been investigated with surprisingly higher heat capacity, thermal expansion coefficient and thermal conductivity compared to their counterpart materials due to the strong anisotropic strength as single crystals [60]. The ability to withstand thermal stress depends largely on some thermo-physical and mechanical properties of the prospected materials—Inconel 718, Ti–6Al–4V, Nimonic 80A, NbB_2 and GTD 111 DS alloy. Thermal properties such as thermal conductivity (k) and coefficient of thermal expansion (CTE) have considerable contribution to the generated thermal stress upon the stator blade and so they are presented in Figs. 4 and 5, respectively, as functions of temperature. Melting point of each material is presented in Table 1. Mechanical properties such as Young's modulus (E) as well as Poisson ratio (σ) also attribute to the generation of

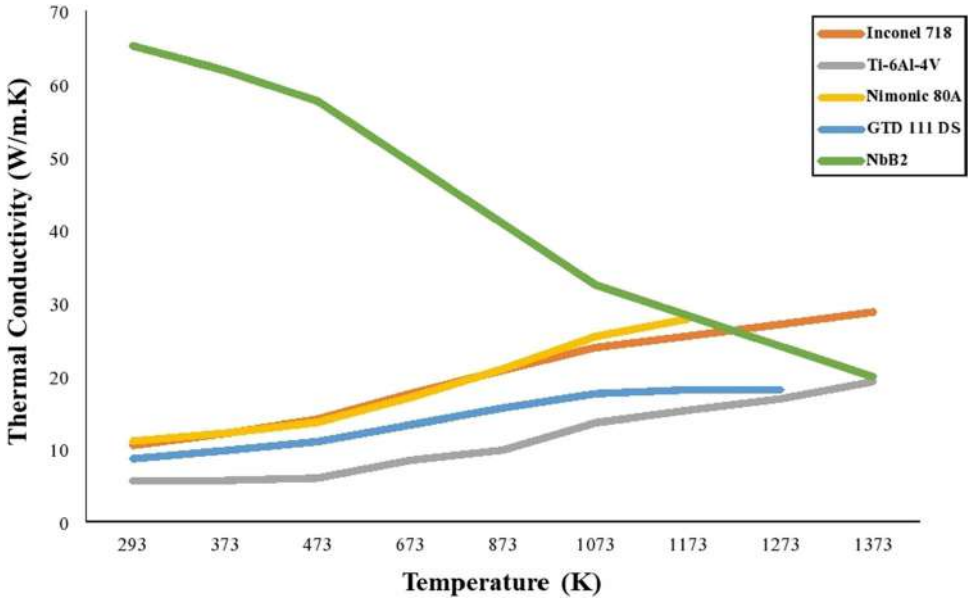

Fig. 4 Thermal conductivity (k) as a function of temperature [61, 62]

thermal strain of a material under hot working condition, which in turn results in thermal stress—making study of both properties pivotal for the current work. Table 2 presents the Young's modulus (E) and Poisson ratio (σ) for the corresponding materials.

Boundary Conditions

Three types of boundary conditions are applied in the present work. Solid mechanics boundary conditions are essential to solve the linear elastic equations, whereas roller and spring boundary conditions are used to define the movement of the blade.

The roller boundary condition limits the movement of the blade in the normal direction of the surface so that the blade can only move in the parallel direction, which is shown in Fig. 6. The roller boundary condition is given by [41]:

$$u.n = 0 \qquad \text{(Eq 13)}$$

here n is the normal vector of the surface and u represents the blade deformations.The spring boundary condition presented in Fig. 7 is in the opposite direction of the roller and confines the top and bottom movements of the stator blade following the Hook's law [41]:

$$\sigma.n = -k_s(u - u_0) \qquad \text{(Eq 14)}$$

here n is the surface normal vector, k_s is the stiffness of the spring foundation, u is the final displacement and u_0 is the initial displacement of the blade. However, the vertical displacement at the leading edge is zero. Except the parts

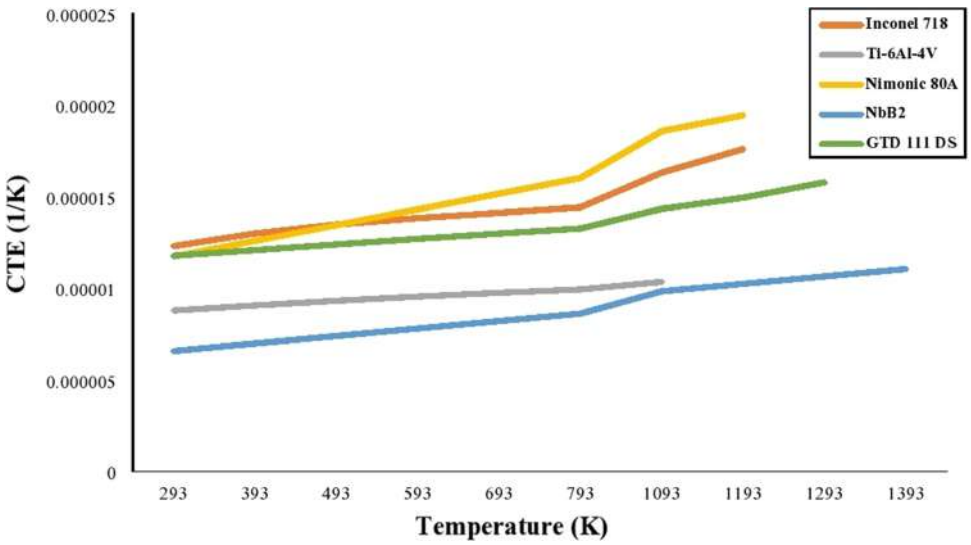

Fig. 5 Coefficient of thermal expansion (CTE) as a function of temperature for the studied materials. [63, 64]

Table 1 Melting points of working materials

Materials	Melting temperature	Ref
Inconel 718	1,533 K	[65]
Ti-6Al-4V	1,877 K	[66]
Nimonic 80A	1,593 K	[67]
NbB_2	3,328 K	[68]
GTD 111 DS	1,523 K	[69]

Table 2 Young's modulus (E) and Poisson ratio (σ) for corresponding materials

Alloy	Young's modulus (GPa)	Poisson ratio	Ref
Inconel 718	199	0.33	[27]
Ti–6Al–4V	105	0.31	[70]
Nimonic 80A	222	0.35	[71]
NbB_2	512	0.22	[72, 73]
GTD 111 DS	128	0.39	[74]

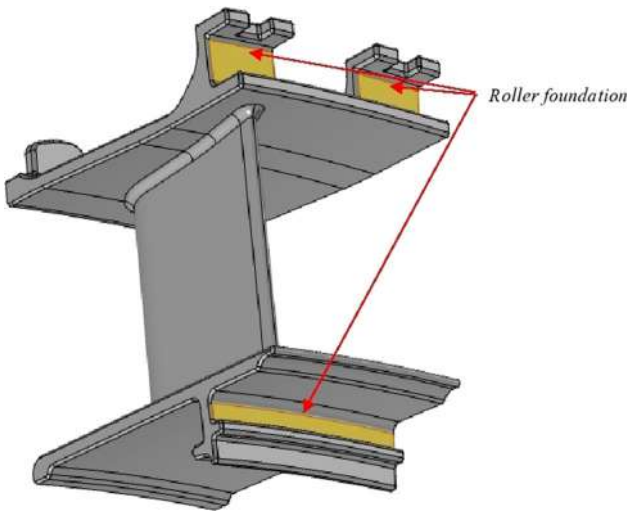

Fig. 6 Roller boundary condition of the stator blade

related to these three boundary conditions all other surfaces of the blade stator are taken under free boundary condition to deform independently during thermal expansion.

The hot combustion gas passes over the blade surface with temperature around 1100 K and a pressure of 30 bar. The velocity of the upper surface of the blade (suction side), the lower surface (pressure side) and the platform walls are taken as 300, 450 and 350 m/s, respectively. It is to be noted that sound speed is taken about 650 m/s and the Mach number for concave and convex sides are approximately 0.7 and 0.45, respectively, which results the air flow into a subsonic flow. The convective heat transfer coefficients can be calculated by [45]:

$$h = \frac{k}{x}\mathrm{Pr}^{\frac{1}{3}} * \left\{ \begin{array}{l} 0.332\mathrm{Re}_x^{\frac{1}{2}} \mathrm{Re}_x \leq 5 * 10^5 \\ 0.0296\mathrm{Re}_x^{\frac{4}{5}} \mathrm{Re}_x \geq 5 * 10^5 \end{array} \right\} \quad \text{(Eq 15)}$$

here k is the conductive heat transfer coefficient, $x(m)$ indicates the distance from the beginning of the plate, Re_x represents the Reynolds number, Pr is the Prandtl number—a dimensionless parameter used in the calculation of heat transfer between a solid body and a moving fluid.

The local working temperature is taken as 900 K, and the convective heat transfer coefficient is 25 W/(m^2 K) calculated from Eq 15. The heat flux of the blade surfaces is determined using the convective heat transfer coefficient Eq 16. The necessary assumption regarding this is that—the pressure and suction sides of the blade are taken as two flat plates employing the local heat transfer coefficient for external forced convection. Also, for maintaining simplicity in calculation of the heat flux for the cooling ducts, the average Nusselt number is taken as Nu = 400 [45]. Thus, the heat flux can be calculated from:

$$q'' = \frac{\mathrm{Nu}_{\mathrm{cool}}\ \mu_{\mathrm{cool}}\ C_{\mathrm{cool}}}{2\,\mathrm{Pr}_{\mathrm{cool}}\ H_{\mathrm{cool}}}(T_{\mathrm{cool}} - T) \quad \text{(Eq 16)}$$

here C indicates the heat capacity in (J/kg K), μ is the viscosity and H defines the characteristic length of cooling air. The insulated boundaries of the stator blade are shown in Fig. 8.

Validation and Mesh Independence

First of all, the fidelity of the numerical model was tested against the available data presented in Vaferi et al. [8]. Secondly, an incisive mesh intendency test was carried out with three different unstructured tetrahedral elements. Table 3 corresponds to a tabular representation of the present study and the numerical values that have been obtained from Vaferi et al. [8]. The proposed numerical model shows much proximity with the validated literature work, which proves its accuracy. Table 4 represents the grid independence test and the outcome of the present work along with the associated errors obtained for three different applied grids. Based on the computational findings, it can be observed that the errors for different element numbers corresponding to the developed thermal stress are 1.172%, 1.147 and 1.150% when compared with the literature data. A more compact and higher accuracy can be seen in case of thermal displacement reducing from 0.20 to 0.203% and further to 0.2033% as the number of meshing elements increases. The errors associated with thermal gradient are little when compared to the literature work showing maximum error of 0.988% to a minimum of 0.9832%.

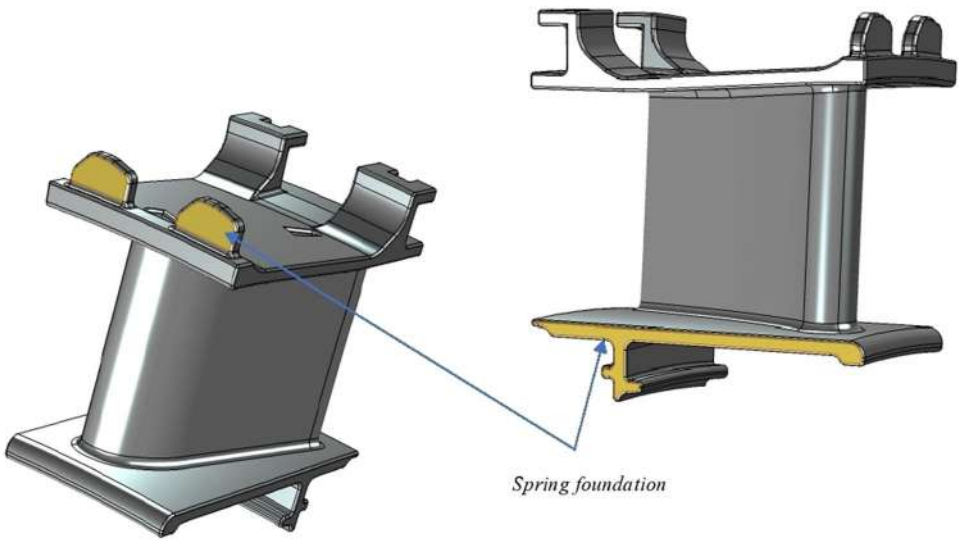

Fig. 7 Spring boundary conditions for the stator blade

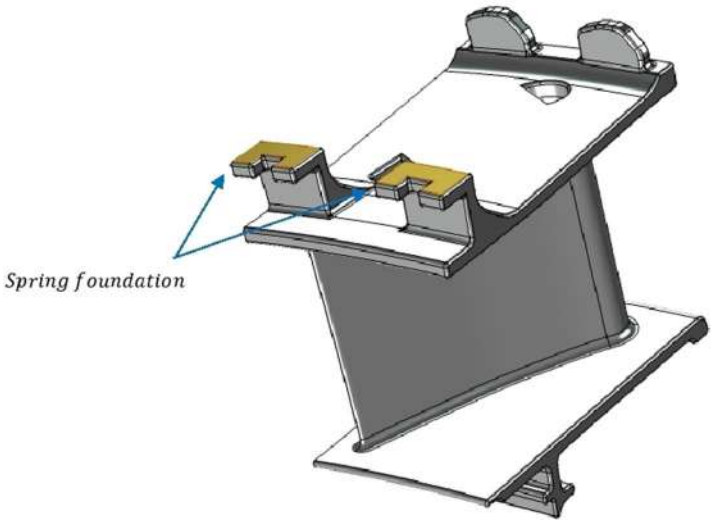

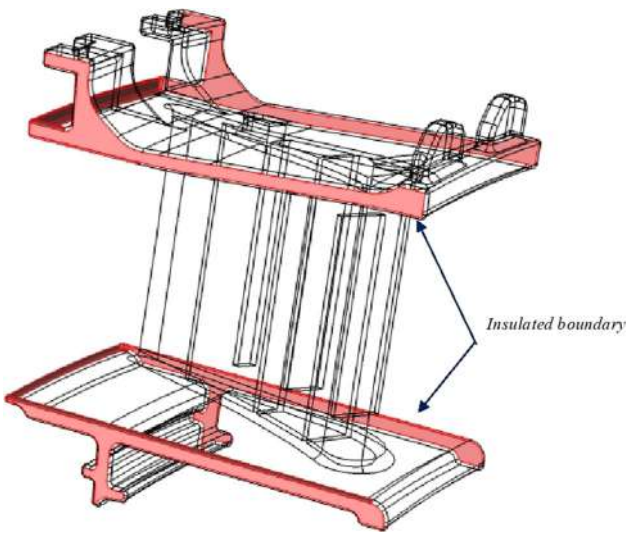

Fig. 8 Insulated boundaries of the stator blade

Figure 9 provides the discretized unstructured free tetrahedral domain that was generated by a commercial finite element analysis (FEA) software. The mesh independence test was conducted using TiB_2 as the stator blade material. It can be seen from the grid independence study that—at each level the associated error is lesser than the earlier level—less than 0.06, 0.003 and 0.14% for thermal gradient, thermal stress and thermal displacement, respectively, when the grid contained more than 1.8 million elements. Table 5 denotes the qualitative statistics of the different applied grids. As per the presented outcomes, it is to be noted that higher number of meshing elements results in improved average element quality of the domain. Mesh independency was obtained by 1867696 elements with an average element quality of 0.8782 and so this grid is selected for further analysis of the study.

Table 3 Tabular comparison between present work and literature [8], TiB_2 as stator blade material

Thermal stress [present]	Thermal stress [75]	Thermal gradient [present]	Thermal gradient [75]	Thermal displacement [present]	Thermal displacement [75]
0.75873	0.75	148.03	149	1.50337	1.5

Table 4 Mesh independence test for applied grids

Elements	Temperature gradient (K)	%, difference	Thermal stress (GPa)	%, difference	Displacement (mm)	%, difference
152068	148.022	0.988	0.7589	1.172	1.503	0.20
185485	148.031	0.9826	0.7587	1.147	1.5033	0.203
1867696	148.0311	0.9832	0.75873	1.15	1.50337	0.2033

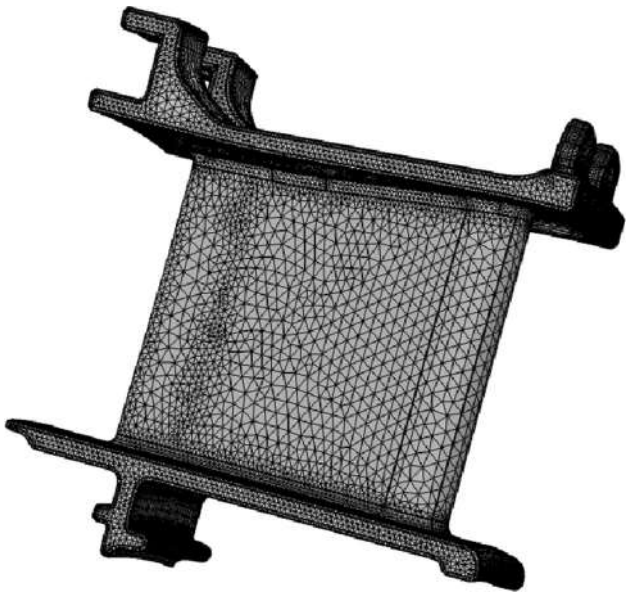

Fig. 9 Applied grid on the turbine stator blade

Table 5 Qualitative analysis of applied three different meshes

Properties	Mesh 1	Mesh 2	Mesh 3
Number of elements	152,068	185,485	1,867,696
Size	Fine	Finer	Extra fine
Average element quality	0.8602	0.8735	0.8782
Minimum element quality	0.2088	0.124	0.0708

Results and Discussion

The prime objective of the proposed study is to investigate the heat transfer behavior of the stator blade due to thermal distribution and acquire the subsequent thermal stress and displacement of the blade. In this section, three deciding parameters of a gas turbine stator blade—thermal dissipation, thermal stress and thermal displacement—that dictate the performance of the turbine compressor under ceaseless and supreme heat transfer condition are computed and compared for five different superalloys and ultra-high-temperature ceramics. Firstly, thermal gradient across the stator blade surface for different superalloys and ceramics is visualized and presented numerically. Secondly, the developed thermal stress due to thermal gradient and thermal expansion at different points of the stator blade structure is analyzed and based on the stress performance analysis highly potential ones are taken into further investigation among the five different materials. A trade-off is observed between thermal gradient and resultant thermal stress of those materials, and this trade-off is explained with their dependence of thermo-physical properties on temperature from the available literature data. Thirdly, magnitude of the thermal displacement due to thermal expansion are computed for all the materials and the areas of the stator blade where the extreme displacements occurred are also showed. Lastly, factor of safety for different materials are calculated under von Mises failure criteria and the material with a combination of—maximum FOS, minimum temperature gradient, thermal stress, and thermal displacement—is proposed as the prospective material for manufacturing stator blade of first-stage gas turbine compressor.

Comparison of Thermal Gradient and Temperature Contours of the Working Stator Blade Materials

This section presents the significance of temperature contours on developing thermal stress as well as comparative analysis of the thermal gradient along the stator blade surface for different materials.

The temperature contours provided in Fig. 10 gives good idea about the temperature gradient at different cross sections of the stator blade structure. Based on these temperature contours and the temperature difference between the blade tip and the adjacent area of the cooling duct, it can be observed that internal cooling through the

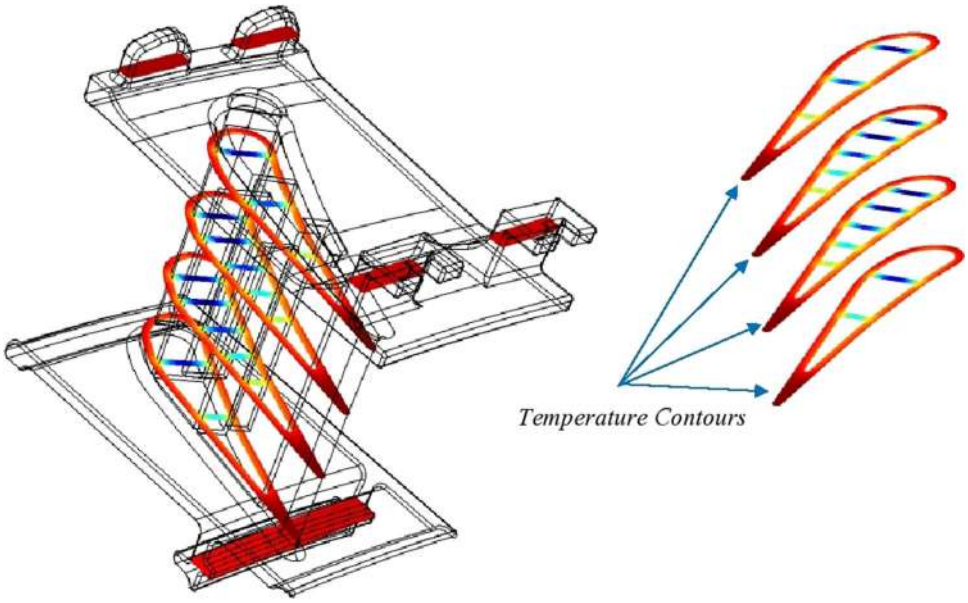

Fig. 10 Temperature contours at different cross sections

cooling duct has a considerable effect on the cooling process of the blade and will help to increase the durability of the blade without compensating the efficiency of the turbine. It is noticed that the temperature gradient is much higher across the cooling duct than any other portion of the blade. Consequently, it suffers more thermal stress than any other parts of the blade and as a result is more vulnerable to start and propagate cracks in the blade. The temperature distribution in stator blades made of Inconel 718, Ti–6Al–4V, Nimonic 80A, NbB_2 and GTD 111 DS alloys is shown in Fig. 11. Being the hottest part of the blade due to constant exposure to high temperature, the trailing edges and trailing ends stand high chance of failure because of subsequent metallurgical defects [76]. However, the minimum temperature for the showed five blades occurs on the fifth baffle wall (from left) or the first baffle wall (from right) with a substantial variance in their respective magnitude. Table 6 provides better estimation of thermal gradient for each of the five materials. It can be observed that the maximum temperature gradient occurs for the blade made of Ti–6Al–4V. A proximity can be seen for NbB_2 and GTD 111 DS in terms of thermal gradient. Inconel 718 shows moderate thermal gradient under this extreme condition of constant heat exchanging, whereas Nimonic 80A has the lowest temperature gradient compared to the other four materials.

Comparison of the Developed Thermal Stress and its Susceptibility to Thermo-Physical Properties of the Working Materials

Under this section, the developed thermal stresses for the proposed five different materials are presented and compared to identify the material that can withstand extreme thermal condition suffering minimum stress. Upon presenting the obtained data from the current numerical study, the best performing materials among the five superalloys and ceramics are further investigated. From the observation, a contradictory relationship with respect to previously stated one between thermal gradient and thermal stress is evolved for the allying better performing materials—which is later explained.

Comparison of Thermal Stress for the Proposed Materials

Due to constant exposure to excessive hot conditions and continuous thermal exchange between the stator blade and internal cooling duct, thermal gradient is evident along the blade surface, which causes thermal stress. Figure 12 provides the stress contours that give better representation of the stress distribution along different cross sections of the stator blade. The stress seems to be maximum at the cooling ducts through which hot air passes and extreme heat transfer takes place. Figure 13 visualizes the developed thermal stress for five different materials and the points of interests where the maximum stress occurred. Among the proposed materials NbB_2 suffers the highest thermal stress, whereas Ti–6Al–4V has the least. Inconel 718 and Nimonic 80A exhibit the same magnitude of thermal stress. GTD 111 DS shows proximity with Ti–6Al–4V when compared; however, the magnitude of thermal stress is higher for GTD 111 DS alloy.

From the stress performance analysis, it can be observed that Ti–6Al–4V exhibits least possible thermal stress, whereas NbB_2 provides the least thermal gradient. The observation is relatively antithetical with the previously

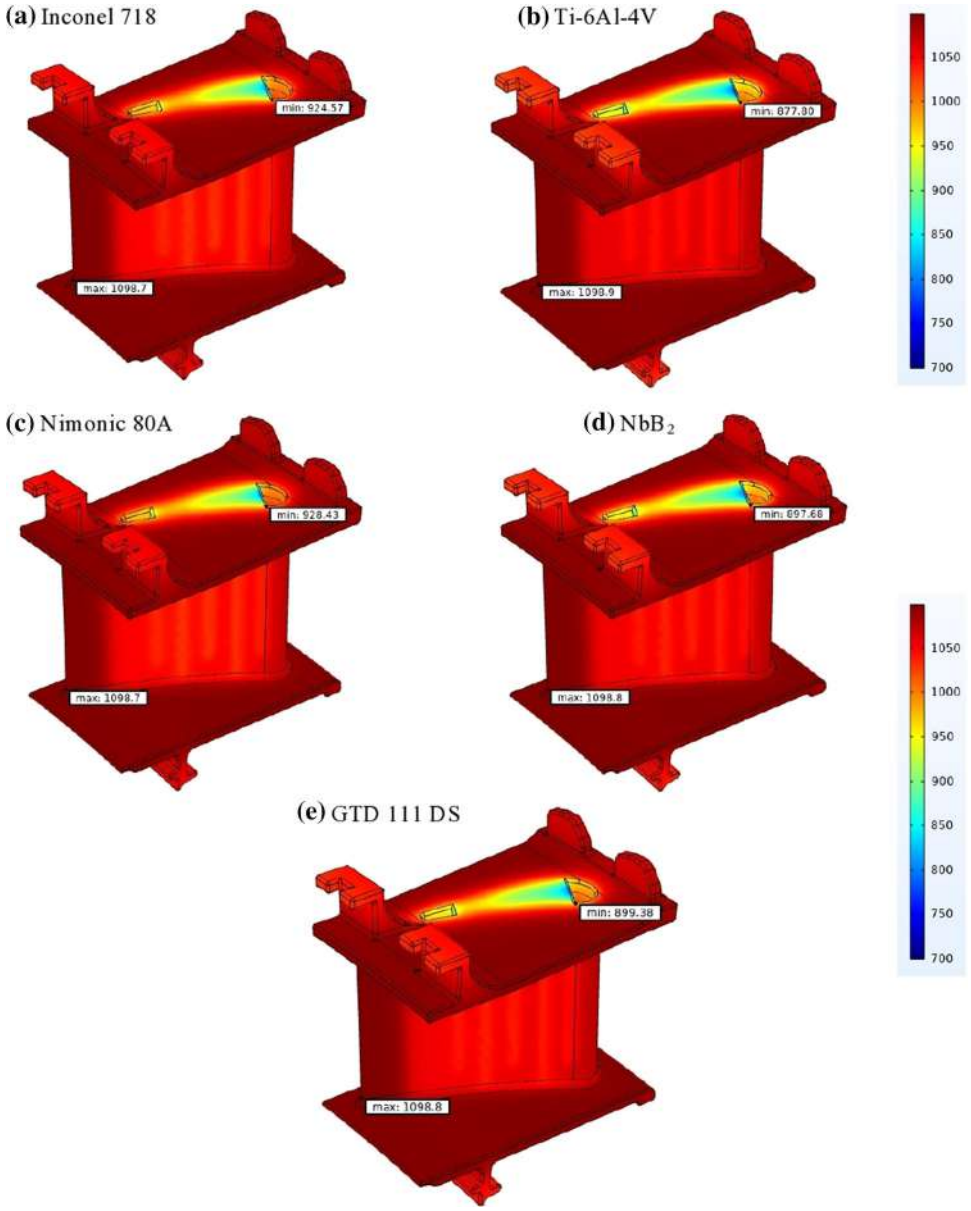

Fig. 11 Temperature distribution (K) in the blades made of Inconel 718, Ti–6Al–4V, Nimonic 80A, NbB_2 and GTD 111 DS

Table 6 Estimated temperature gradient for the working materials

Material	Maximum temperature	Minimum temperature
Inconel 718	1098.7 K	924.57 K
Ti–6Al–4V	1098.9 K	877.80 K
Nimonic 80A	1098.7 K	928.43 K
NbB_2	1098.8 K	897.68 K
GTD 111 DS	1098.8 K	899.38 K

discussed relationship between thermal stress and thermal gradient. This contrasting circumstance can be explained from the dependence of thermo-physical properties on temperature for both Ti–6Al–4V and NbB_2 which is presented in later section.

Exploration of Thermo-Physical Properties of NbB_2 and Ti–6Al–4V at Elevated Temperature and their Effect on Generation of Thermal Stress

The discrepancy between thermal gradient and thermal stress for two of the highly potential materials can be described in terms of the major thermo-physical properties responsible for the generation of thermal stress. Thermal conductivity (k), thermal expansion coefficient (CTE) and Young's modulus (E) are the properties that have been closely observed with respect to increasing temperature above 800 °C for this study. In this section, the most dominating property to cause thermal stress in the stator blade among the previously mentioned thermal properties

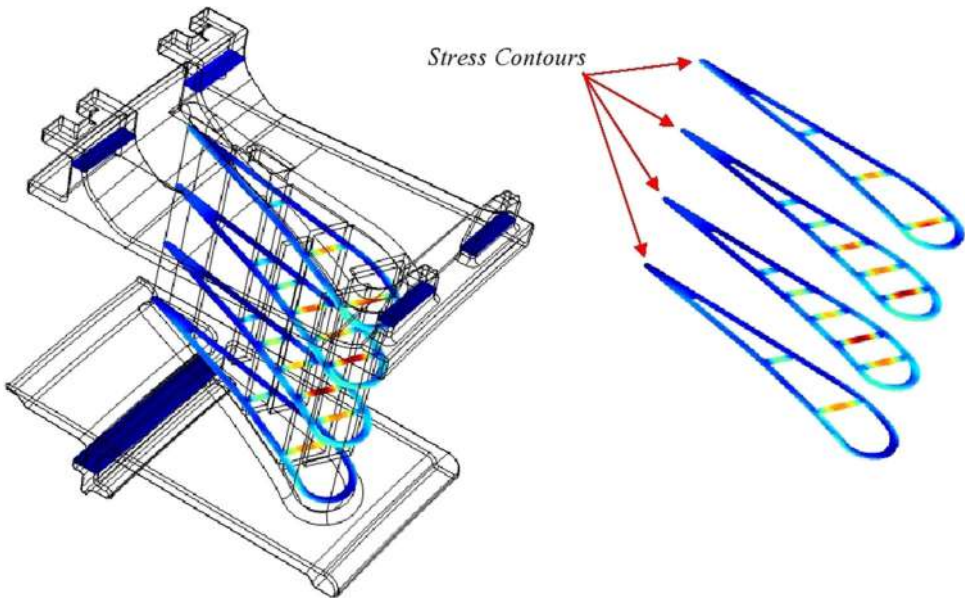

Fig. 12 Thermal stress contours at different cross sections

of the two materials are navigated under the extreme working condition of the gas turbine first-stage compressor.

Proper functioning of the turbine blades at extreme temperature and belated initiation of crack within the blade surface will require materials with higher melting point and ability to sustain in this extreme temperature. From Table 1, it is seen that none of the proposed materials can maintain their solidus phase above 1600 K except Ti–6Al–4V and NbB_2. Taking this point into consideration, both NbB_2 and Ti–6Al–4V are further forwarded to investigate their sustainability as stator blade material under severely hot working condition inside gas turbine compressor. Being an ultra-high-temperature ceramic boride, NbB_2 exhibits excessive temperature resistance [77]. Ti–6Al–4V has slightly higher coefficient of thermal expansion than NbB_2; however, Fig. 14 shows that at elevated temperature above 1373 K Ti–6Al–4V has a positive slope of thermal conductivity, whereas NbB_2 manifests a steep negative slop with respect to temperature. As a result, Ti–6Al–4V has more uniform distribution of heat dissipation over the blade surface than NbB_2 at temperature above 1373 K, which results in lower thermal expansion. Because of this lower thermal expansion, the aftermath thermal stress is much lower for Ti–6Al–4V compared to NbB_2.

At high-temperature condition (above 1373 K), NbB_2 has much higher thermal expansion rate as given in Fig. 15 and so during the extreme heating condition in the compressor—coefficient of thermal expansion of NbB_2 becomes more evident than its thermal conductivity. Thermal conductivity (k) of NbB_2 is much lower in high thermal condition and that is why the developed stress within the NbB_2 stator is attributed to its high coefficient of thermal expansion (CTE) rather than low thermal conductivity, whereas the thermal stress of Ti–6Al–4V stator blade corresponds to its high thermal conductivity at elevated temperature rather than its low thermal expansion coefficient. Another fact to be noted that Ti–6Al–4V has much lower Young's modulus than NbB_2, which also corresponds to lower thermal stress as given in Table 2. It can be estimated from the discussion that both thermal conductivity and Young's modulus of the respective materials have better impact on the developed stress than the coefficient of thermal expansion.

Comparison of Thermal Displacement for the Working Materials

This section represents the developed thermal displacement, which is due to thermal stress and thermal gradient along the stator blade surface. Maximum and minimum displacements for all the five materials are presented, and the overall effect of thermal gradient on generating thermal stress is also briefly explained under this subsection.

Figure 16 demonstrates the maximum and minimum displacement for the respective materials. Inconel 718, Nimonic 80A and GTD 111 DS have higher thermal displacement compared to the other two materials with magnitude of 3.2 mm, 3.0 mm and 3.0 mm. On the other hand, Ti–6Al–4V and NbB_2 exhibited relatively lower thermal displacement with magnitude of 2.2 and 1.5 mm sequentially. An interesting point of discussion could be the difference of maximum and minimum thermal displacement, which gives a better overview of the thermal expansion of the stator blades due to heavy heat flux generation. Table 7 provides the difference between maximum and minimum thermal displacement of stator blade

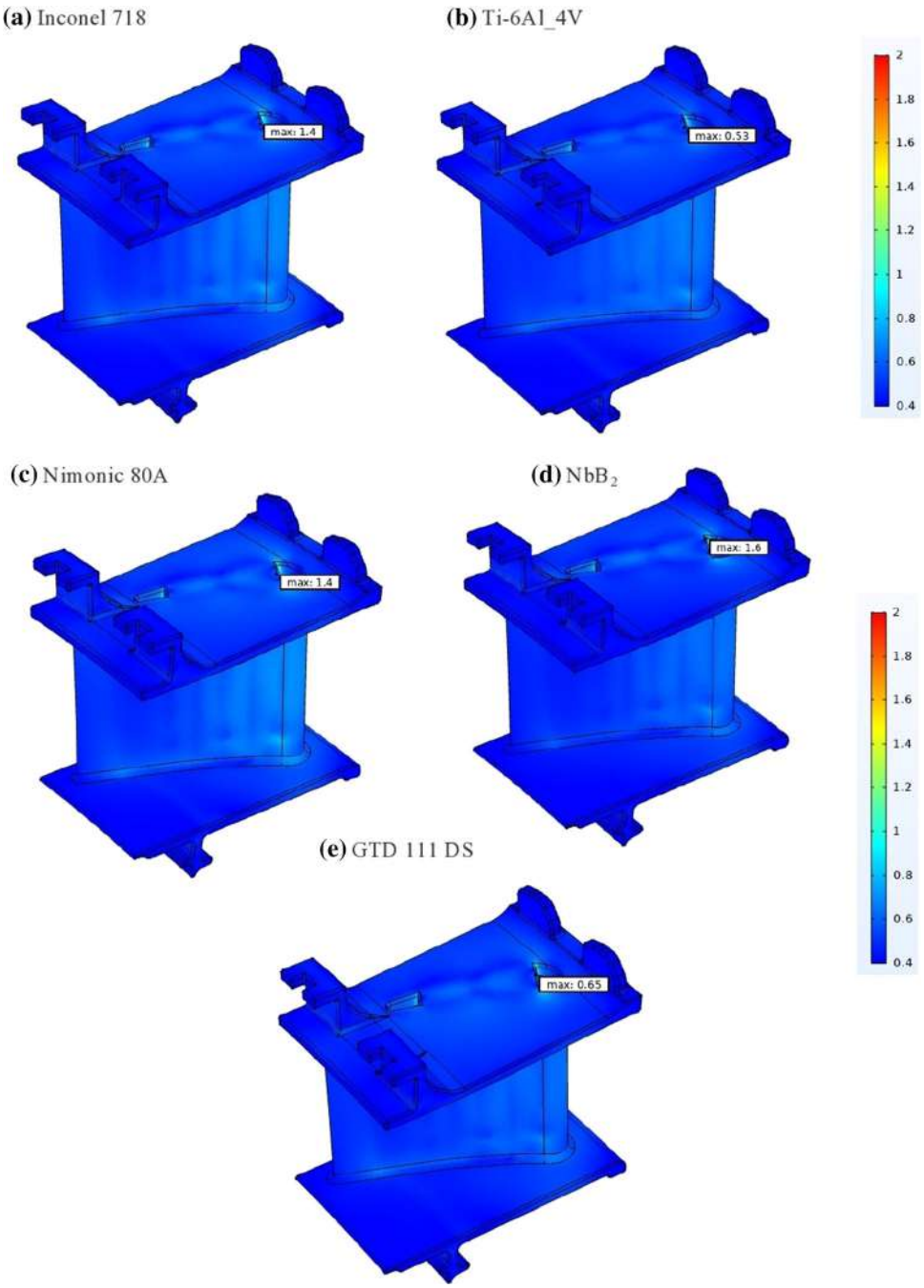

Fig. 13 Thermal stress (GPa) distribution in the blades made of Inconel 718, Ti–6Al–4V, Nimonic 80A, NbB_2 and GTD 111 DS

made of five materials. It is to be observed that Ti–6Al–4V and GTD 111 DS have the least effect of thermal expansion with displacement difference of 2.148 and 1.36 mm. Nimonic 80A, Inconel 718 and NbB_2 have relatively higher effect of thermal expansion with magnitude of 2.65, 2.82 and 2.76 mm, respectively. Higher thermal expansion corresponds to inefficient dissipation of heat along the blade surface and thereby causes higher thermal gradient. This higher thermal gradient results in more thermal displacement. Displacement contours for different cross sections are provided in Fig. 17. Minimum displacement for the materials occurs at the insulation wall and the trailing edges, whereas it increases and becomes maximum at the leading edges of the blade. Spring and roller foundations cause minimum displacement from the upper surface of the blade to the insulation wall.

Comparison of Safety Factor (FOS) for All the Applied Materials.

The safety factor of the stator blade made of the proposed materials is important to understand whether the material

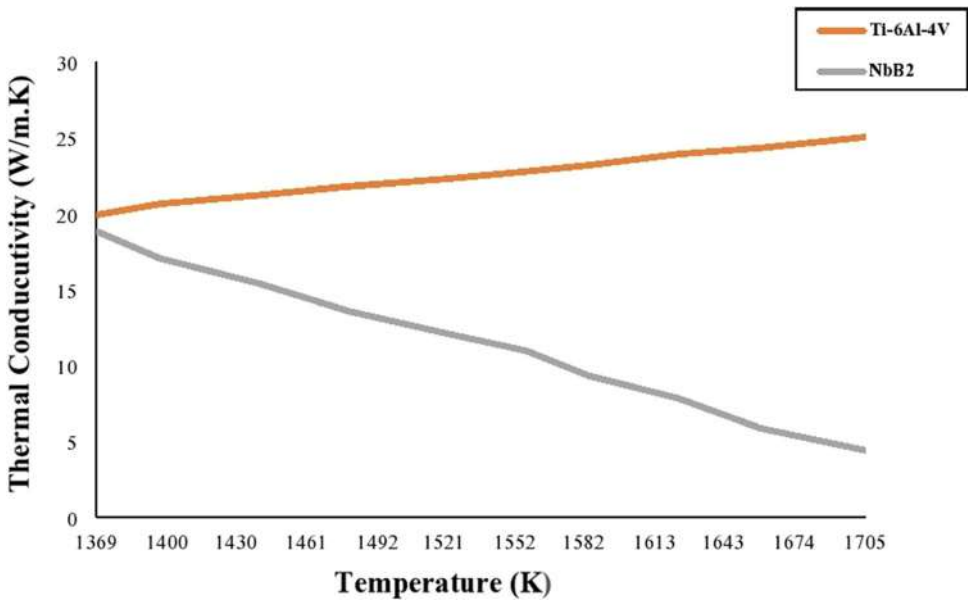

Fig. 14 Thermal conductivity as function of elevated temperature for Ti–6Al–4V and NbB2 [64, 78]

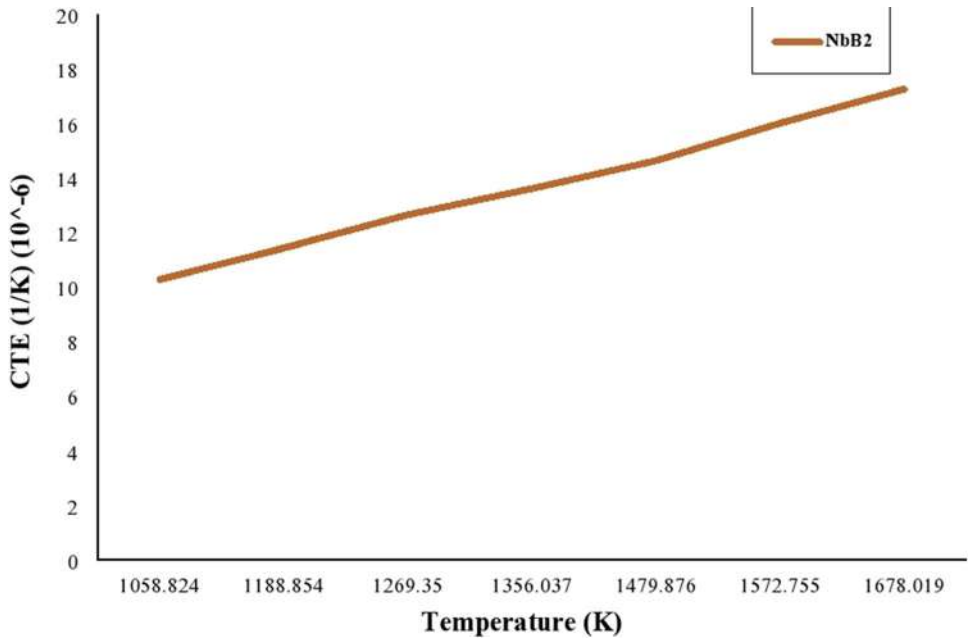

Fig. 15 Coefficient of thermal expansion (CTE) of NbB_2 as a function of elevated temperature above 800 °C [79]

can withstand the developed thermal stress under extreme heat exchanging condition or not. The FOS (Factor of safety) for all the superalloys and ultra-high-temperature ceramic are calculated in this section of the paper. For calculation purpose—ultimate strengths of the materials are taken into consideration from available literature data and then compared with the developed thermal stress within the blade surface. Upon obtaining the FOS, the results are compared among the applied materials. The total calculation of factor of safety for the materials is done considering minimum safety limit of 1.2 under von Mises failure theory.

Table 8 provides the safety factor of the five materials. As mentioned earlier, thermal conductivity and thermal expansion along with Young's modulus have huge contribution to the developed thermal stress in the blade material. Maintaining coherence with this hypothesis, the numerical results provide optimum safety factor of 1.83 for Ti–6Al–4V, whereas NbB_2 and GTD 111 DS alloy can barely withstand the stress with a safety factor of 1.00 even though NbB_2 has the highest compressive strength of 1.5 GPa [80] compared to the other four materials. Inconel 718 and Nimonic 80A have safety factor of 0.785 and 0.55, respectively, indicating probable failure of the blade under

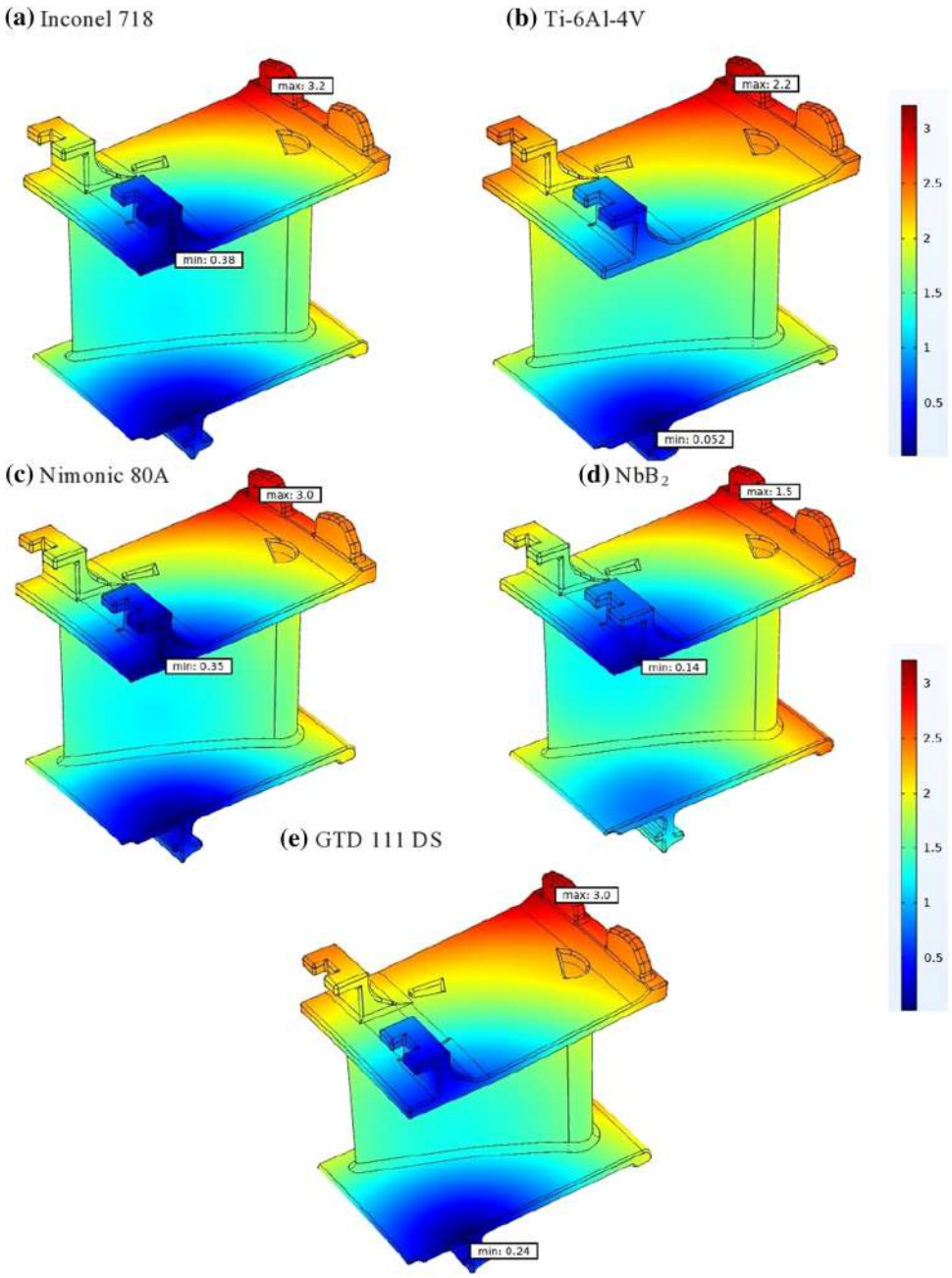

Fig. 16 Displacement distribution (mm) in the blades made of Inconel 718, Ti–6Al–4V, Nimonic 80A, NbB_2 and GTD 111 DS

Table 7 Difference between maximum and minimum thermal displacements for the working materials

Materials	Maximum thermal displacement (mm)	Minimum thermal displacement (mm)	Difference
Inconel 718	3.2	0.38	2.82
Ti–6Al–4V	2.2	0.052	2.148
Nimonic 80A	3.0	0.35	2.65
GTD 111 DS	1.5	0.14	1.36
NbB_2	3.0	0.24	2.76

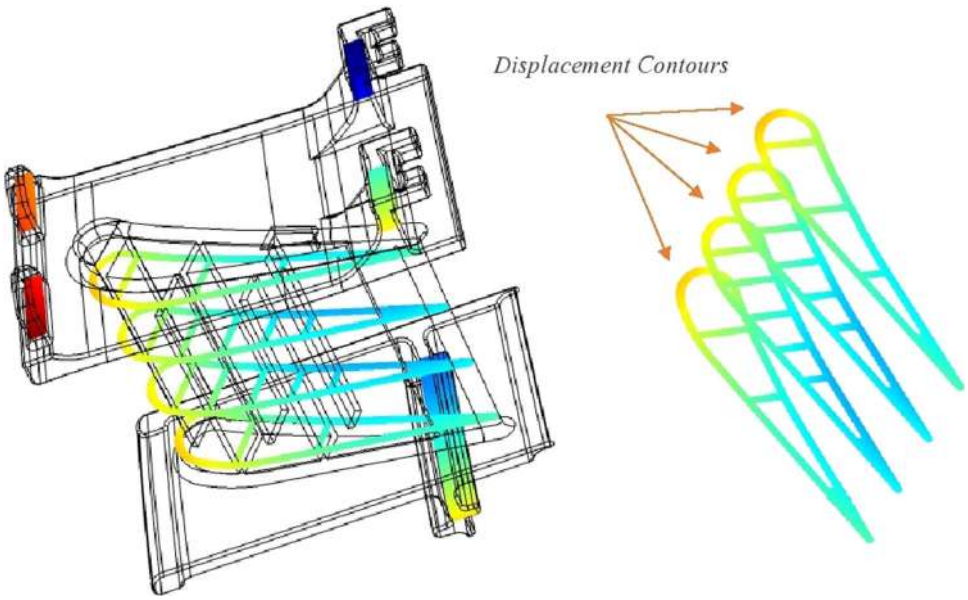

Fig. 17 Displacement contours at different cross sections

Table 8 Factor of safety for all the working materials

Material	Inconel 718	Ti–6Al–4V	Nimonic 80A	NbB_2	GTD 111 DS
Yield strength (MPa)	1100	970	780	1500	645.2
Safety factor	0.785	1.83	0.55	1.00	1.00

extreme condition having ultimate strength of 1.1 and 0.78 GPa, respectively [81–83].

Conclusions

Presented numerical work evaluates the potential use of superalloys and ceramic materials—Inconel 718, Ti–6Al–4V, Nimonic 80A, NbB_2 and GTD 111 DS as gas turbine stator blade material without total rupture of the system. The probability of failure for all the materials has been investigated under the von Mises criteria considering the thermal stress. Although Coulomb–Mohr criteria is good for predicting failure in brittle materials such as—NbB_2, von Mises criteria provide better failure approximation for both brittle and ductile materials and so this failure criterion is incorporated for the work to do a comprehensive comparative analysis. From the numerical report, it is to be observed that Inconel 718 and Nimonic 80A have factor of safety less than 1 predicting probable failure under the thermal stress. Between NbB_2 and GTD 111 DS—NbB_2 has lower thermal displacement even after having approximately similar FOS to GTD 111 DS under extreme thermal condition. However, Ti–6Al–4V provides better

functionality than NbB_2 with higher safety factor and a moderate compensation in thermal displacement—concluding Ti–6Al–4V as the suitable material for manufacturing gas turbine stator blade.

Acknowledgments To acknowledge the contribution of Monazat E Jannat and Reaz Chaklader to the overall successful completion of the project, the author would like to express their gratitude. This research did not receive any specific grant from funding agencies in the public, commercial, or not-for-profit sectors.

Authors Contribution AA did conceptualization, validation, formal analysis, visualization, writing—original draft, writing—review and editing, software. MTS was involved in supervision, data curation, review, and editing.

Conflict of interest The authors declare that they have no known competing financial interests or personal relationships that could have appeared to influence the work reported in this paper.

References

1. Y. Liu, Y. Zhou, W. Wu, Assessing the impact of population, income and technology on energy consumption and industrial pollutant emissions in China. Appl. Energy. **155**, 904–917 (2015). https://doi.org/10.1016/j.apenergy.2015.06.051
2. B. Mullan, J. Haqq-Misra, Population growth, energy use, and the implications for the search for extraterrestrial intelligence. Futures. **106**, 4–17 (2019). https://doi.org/10.1016/j.futures.2018.06.009
3. T. Gholizadeh, M. Vajdi, H. Rostamzadeh, Exergoeconomic optimization of a new trigeneration system driven by biogas for power, cooling, and freshwater production. Energy Convers. Manag. **205**, 112417 (2020). https://doi.org/10.1016/j.enconman.2019.112417
4. T. Gholizadeh, M. Vajdi, H. Rostamzadeh, A new trigeneration system for power, cooling, and freshwater production driven by a flash-binary geothermal heat source. Renew. Energy. **148**, 31–43 (2020). https://doi.org/10.1016/j.renene.2019.11.154
5. T.T. Chow, A review on photovoltaic/thermal hybrid solar technology. Appl. Energy. **87**(2), 365–379 (2010). https://doi.org/10.1016/j.apenergy.2009.06.037
6. D.O. Hall, Biomass energy. Energy Policy. **19**(8), 711–737 (1991). https://doi.org/10.1016/0301-4215(91)90042-M
7. M. A. Boles and Y. A. Çengel, *Thermodyn. Eng. Approach*. (2015)
8. K. Vaferi et al., Heat transfer, thermal stress and failure analyses in a TiB_2 gas turbine stator blade. Ceram. Int. **45**(15), 19331–19339 (2019). https://doi.org/10.1016/j.ceramint.2019.06.184
9. D.B. Kang, S.W. Lee, Effects of squealer rim height on heat/mass transfer on the floor of cavity squealer tip in a high turning turbine blade cascade. Int. J. Heat Mass Transf. **99**, 283–292 (2016). https://doi.org/10.1016/j.ijheatmasstransfer.2016.03.121
10. M.W. Benner, S.A. Sjolander, S.H. Moustapha, An empirical prediction method for secondary losses in turbines: part II—a new secondary loss correlation. J. Turbomach. **128**(2), 281–291 (2006). https://doi.org/10.1115/1.2162594
11. S.W. Lee, J.S. Joo, Heat/mass transfer over the cavity squealer tip equipped with a full coverage winglet in a turbine cascade: part 2—data on the cavity floor. Int. J. Heat Mass Transf. **108**, 1264–1272 (2017). https://doi.org/10.1016/j.ijheatmasstransfer.2016.12.026
12. J. Hou, B.J. Wicks, R.A. Antoniou, An investigation of fatigue failures of turbine blades in a gas turbine engine by mechanical analysis. Eng. Fail. Anal. **9**(2), 201–211 (2002). https://doi.org/10.1016/S1350-6307(01)00005-X
13. J.S. Park, W. Choi, Heat and mass transfer characteristics on the first-stage gas turbine blade under unsteady wake flow. Int. J. Therm. Sci. **138**, 314–321 (2019). https://doi.org/10.1016/j.ijthermalsci.2019.01.008
14. S. Qu, C.M. Fu, C. Dong, J.F. Tian, Z.F. Zhang, Failure analysis of the 1st stage blades in gas turbine engine. Eng. Fail. Anal. **32**, 292–303 (2013). https://doi.org/10.1016/j.engfailanal.2013.03.017
15. M. Rezazadeh Reyhani, M. Alizadeh, A. Fathi, H. Khaledi, Turbine blade temperature calculation and life estimation: a sensitivity analysis. Propuls. Power Res. **2**(2), 148–161 (2013). https://doi.org/10.1016/j.jppr.2013.04.004
16. S. Zecchi, L. Arcangeli, B. Facchini, D. Coutandin, 2004, Features of a cooling system simulation tool used in industrial preliminary design stage". Proc. ASME Turbo Expo. **3**, 493–501 (2004). https://doi.org/10.1115/gt2004-53547
17. D. Coutandin, S. Taddei, B. Facchini, Advanced doublewall cooling system development for turbine vanes. Proc. ASME Turbo Expo. **3**, 623–632 (2006). https://doi.org/10.1115/GT2006-90784
18. A. Sato, Y.L. Chiu, R.C. Reed, Oxidation of nickel-based single-crystal superalloys for industrial gas turbine applications. Acta Mater. **59**(1), 225–240 (2011). https://doi.org/10.1016/j.actamat.2010.09.027
19. R.E. Schafrik, R. Sprague, Gas turbine materials. Adv. Mater. Process. **162**(6), 41–46 (2004). https://doi.org/10.1016/0016-0032(58)90740-3
20. G.M.M.B. Henderson, D. Arrell, M. Heobel, R. Larsson, Nickel-based superalloy welding practices for industrial gas turbine applications. Sci. Technol. Weld. Join. **9**(1), 1–14 (2004)
21. Y.H. Wen, B. Wang, J.P. Simmons, Y. Wang, A phase-field model for heat treatment applications in Ni-based alloys. Acta Mater. **54**(8), 2087–2099 (2006). https://doi.org/10.1016/j.actamat.2006.01.001
22. M. Kliuev et al., EDM drilling and shaping of cooling holes in inconel 718 turbine blades. Procedia CIRP. **42**, 322–327 (2016). https://doi.org/10.1016/j.procir.2016.02.293
23. S. Roy, R. Kumar, A.. P. Anurag, R.K. Das, A brief review on machining of inconel 718. Mater. Today Proc. **5**(9), 18664–18673 (2018). https://doi.org/10.1016/j.matpr.2018.06.212
24. A. Thomas, M. El-Wahabi, J.M. Cabrera, J.M. Prado, High temperature deformation of Inconel 718. J. Mater. Process. Technol. **177**(1–3), 469–472 (2006). https://doi.org/10.1016/j.jmatprotec.2006.04.072
25. E. Hosseini, V.A. Popovich, A review of mechanical properties of additively manufactured Inconel 718. Addit. Manuf. **30**, 100877 (2019). https://doi.org/10.1016/j.addma.2019.100877
26. X. Wang, X. Gong, K. Chou, Review on powder-bed laser additive manufacturing of Inconel 718 parts. Proc. Inst. Mech. Eng. Part B J. Eng. Manuf. **231**(11), 1890–1903 (2017). https://doi.org/10.1177/0954405415619883
27. W. Maktouf, K. Saï, An investigation of premature fatigue failures of gas turbine blade. Eng. Fail. Anal. **47**, 89–101 (2015). https://doi.org/10.1016/j.engfailanal.2014.09.015
28. M. Peters, J. Kumpfert, C.H. Ward, C. Leyens, Titanium alloys for aerospace applications. Adv. Eng. Mater. **5**(6), 419–427 (2003). https://doi.org/10.1002/adem.200310095
29. J.C. Williams, R.R. Boyer, Opportunities and issues in the application of titanium alloys for aerospace components. Metals (Basel). (2020). https://doi.org/10.3390/met10060705

30. A. Kermanpur, H. Sepehri Amin, S. Ziaei-Rad, N. Nourbakhshnia, M. Mosaddeghfar, Failure analysis of Ti6Al4V gas turbine compressor blades. Eng. Fail. Anal. **15**(8), 1052–1064 (2008). https://doi.org/10.1016/j.engfailanal.2007.11.018
31. S. Luo, D. Zhu, L. Hua, D. Qian, S. Yan, F. Yu, Effects of process parameters on deformation and temperature uniformity of forged Ti–6Al–4V turbine blade. J. Mater. Eng. Perform. **25**(11), 4824–4836 (2016). https://doi.org/10.1007/s11665-016-2320-0
32. J.R. Scheibel, R. Aluru, H. van Esch, "Mechanical properties in GTD-111 alloy in heavy frame gas turbines. Am. Soc. Mech. Eng. (2018). https://doi.org/10.1115/GT2018-75432
33. K. Sabri, M. Gaceb, M.O. Si-Chaib, Analysis of a directionally solidified (DS) GTD-111 turbine blade failure. J. Fail. Anal. Prev. **20**(4), 1162–1174 (2020). https://doi.org/10.1007/s11668-020-00920-y
34. A.A. Pauzi, N. Berahim, S. Husin, Degradation of gas turbine blades for a thermal power plant. MATEC Web Conf. **54**, 6–9 (2016). https://doi.org/10.1051/matecconf/20165403002
35. W.G. Fahrenholtz, G.E. Hilmas, I.G. Talmy, J.A. Zaykoski, Refractory diborides of zirconium and hafnium. J. Am. Ceram. Soc. **90**(5), 1347–1364 (2007). https://doi.org/10.1111/j.1551-2916.2007.01583.x
36. S. Zhu, W.G. Fahrenholtz, G.E. Hilmas, Influence of silicon carbide particle size on the microstructure and mechanical properties of zirconium diboride-silicon carbide ceramics. J. Eur. Ceram. Soc. **27**(4), 2077–2083 (2007). https://doi.org/10.1016/j.jeurceramsoc.2006.07.003
37. M.S. Asl, M.G. Kakroudi, B. Nayebi, H. Nasiri, Taguchi analysis on the effect of hot pressing parameters on density and hardness of zirconium diboride. Int. J. Refract. Met. Hard Mater. **50**, 313–320 (2015). https://doi.org/10.1016/j.ijrmhm.2014.09.006
38. R. Königshofer et al., Solid-state properties of hot-pressed TiB_2 ceramics. Int. J. Refract. Met. Hard Mater. **23**(4–6), 350–357 (2005). https://doi.org/10.1016/j.ijrmhm.2005.05.006
39. M. Vajdi, F.S. Moghanlou, Z. Ahmadi, A. Motallebzadeh, M. Shahedi Asl, Thermal diffusivity and microstructure of spark plasma sintered TiB_2 [sbnd] SiC [sbnd] Ti composite. Ceram. Int. **45**(7), 8333–8344 (2019). https://doi.org/10.1016/j.ceramint.2019.01.141
40. S. Nekahi, K. Vaferi, M. Vajdi, F.S. Moghanlou, M.S. Asl, M. Shokouhimehr, A numerical approach to the heat transfer and thermal stress in a gas turbine stator blade made of HfB_2. Ceram. Int. **45**(18), 24060–24069 (2019). https://doi.org/10.1016/j.ceramint.2019.08.112
41. F.S. Moghanlou, M. Vajdi, A. Motallebzadeh, J. Sha, M. Shokouhimehr, M.S. Asl, Numerical analyses of heat transfer and thermal stress in a ZrB_2 gas turbine stator blade. Ceram. Int. **45**(14), 17742–17750 (2019). https://doi.org/10.1016/j.ceramint.2019.05.344
42. M.S. Asl, B. Nayebi, M. Shokouhimehr, TEM characterization of spark plasma sintered ZrB_2–SiC–graphene nanocomposite. Ceram. Int. **44**(13), 15269–15273 (2018). https://doi.org/10.1016/j.ceramint.2018.05.170
43. M.S. Asl, B. Nayebi, A. Motallebzadeh, M. Shokouhimehr, Nanoindentation and nanostructural characterization of ZrB_2–SiC composite doped with graphite nano-flakes. Compos. Part B Eng. **175**, 107–153 (2019). https://doi.org/10.1016/j.compositesb.2019.107153
44. M. Mallik, A.J. Kailath, K.K. Ray, R. Mitra, Electrical and thermophysical properties of ZrB_2 and HfB_2 based composites. J. Eur. Ceram. Soc. **32**(10), 2545–2555 (2012). https://doi.org/10.1016/j.jeurceramsoc.2012.02.013
45. K. Vaferi et al., Thermo-mechanical simulation of ultrahigh temperature ceramic composites as alternative materials for gas turbine stator blades. Ceram. Int. **47**(1), 567–580 (2021). https://doi.org/10.1016/j.ceramint.2020.08.164
46. M. Usta, The characterization of borided pure niobium. Surf. Coat. Technol. **194**(2–3), 251–255 (2005). https://doi.org/10.1016/j.surfcoat.2004.06.040
47. M. Usta, I. Ozbek, C. Bindal, A.H. Ucisik, S. Ingole, H. Liang, A comparative study of borided pure niobium, tungsten and chromium. Vacuum. **80**(11–12), 1321–1325 (2006). https://doi.org/10.1016/j.vacuum.2006.01.036
48. Ö. Balcı, D. Ağaoğulları, F. Muhaffel, M.L. Öveçoğlu, H. Çimenoğlu, İ Duman, Effect of sintering techniques on the microstructure and mechanical properties of niobium borides. J. Eur. Ceram. Soc. **36**(13), 3113–3123 (2016). https://doi.org/10.1016/j.jeurceramsoc.2016.05.014
49. Y. Xu et al., Strengthening mechanisms of carbon in modified nickel-based superalloy Nimonic 80A. Mater. Sci. Eng. A. **528**(13–14), 4600–4607 (2011). https://doi.org/10.1016/j.msea.2011.02.072
50. M. Bahgat, M.K. Paek, C.H. Park, J.J. Pak, Thermal synthesis of nanocrystalline ($CoxNi_1$-x) yFe_1-y KOVAR alloy through gaseous reduction of mixed oxides. Mater. Trans. **49**(1), 208–214 (2008). https://doi.org/10.2320/matertrans.MER2007229
51. A. Günen, K.M. Döleker, M.E. Korkmaz, M.S. Gök, A. Erdogan, Characteristics, high temperature wear and oxidation behavior of boride layer grown on nimonic 80A Ni-based superalloy. Surf. Coat. Technol. **409**, 126906 (2021). https://doi.org/10.1016/J.SURFCOAT.2021.126906
52. M.E. Korkmaz, N. Yaşar, M. Günay, Numerical and experimental investigation of cutting forces in turning of Nimonic 80A superalloy. Eng. Sci. Technol. Int. J. **23**(3), 664–673 (2020). https://doi.org/10.1016/j.jestch.2020.02.001
53. D.K. Kim, D.Y. Kim, S.H. Ryu, D.J. Kim, Application of nimonic 80A to the hot forging of an exhaust valve head. J. Mater. Process. Technol. **113**(1–3), 148–152 (2001). https://doi.org/10.1016/S0924-0136(01)00700-2
54. R.R. Kumar, K.M. Pandey, Static structural and modal analysis of gas turbine blade. IOP Conf. Ser. Mater. Sci. Eng. **225**(1), 0–9 (2017). https://doi.org/10.1088/1757-899X/225/1/012102
55. H. Khawaja, M. Moatamedi, Selection of high performance alloy for gas turbine blade using multiphysics analysis. Int. J. Multiphys. **8**(1), 91–100 (2014). https://doi.org/10.1260/1750-9548.8.1.91
56. R. Subbarao, N. Mahato, Computational analysis on the use of various nimonic alloys as gas turbine blade materials. Gas Turbine India Conf. (2019). https://doi.org/10.1115/GTINDIA2019-2398
57. P. Taylor, Machining science and technology: an international machinability of nickel-based high temperature alloys. Mach. Sci. Technol. Int. J. **4**(1), 37–41 (2014)
58. C. Carcasci, B. Facchini, A numerical procedure to design internal cooling of gas turbine stator blades. Rev. Gen. Therm. **35**(412), 257–268 (1996). https://doi.org/10.1016/S0035-3159(96)80018-3
59. G. Turbine and S. C. Solid, 2020. Nickel-based superalloys machinability of nickel-based superal- loys: an overview microstructure control in processing nickel, titanium and other special alloys superalloys for gas turbine engines nickel-based superalloys. Mechanical Properties of Mul-T
60. W.G. Fahrenholtz, G.E. Hilmas, Ultra-high temperature ceramics: Materials for extreme environments. Scr. Mater. **129**, 94–99 (2017). https://doi.org/10.1016/j.scriptamat.2016.10.018
61. J.N. Sweet, E.P. Roth, M. Moss, Thermal conductivity of Inconel 718 and 304 stainless steel. Int. J. Thermophys. **8**(5), 593–606 (1987). https://doi.org/10.1007/BF00503645
62. I. Akin, B.Ç. Ocak, F. Sahin, G. Goller, Effects of SiC and SiC–GNP additions on the mechanical properties and oxidation behavior of NbB 2. J. Asian Ceram. Soc. **7**, 1–13 (2019). https://doi.org/10.1080/21870764.2019.1595929

63. C. Street, U.S.A. Mass, T. Losekamp, Review paper: tabulation of the coefficients of a quadratic function for the thermal expansion of various alloys and other engineering materials. Mater Sci. Eng. **10**, 193–203 (1972)
64. L. Metals, Letter A study of the thermal of NbB2 and TaBz*. 139, 7–10, (1988)
65. G.A. Knorovsky, M.J. Cieslak, T.J. Headley, A.D. Romig, W.F. Hammetter, INCONEL 718: a solidification diagram. Metall. Trans. A. **20**(10), 2149–2158 (1989). https://doi.org/10.1007/BF02650300
66. M.K. Lee, J.G. Lee, Mechanical and corrosion properties of Ti–6Al–4V alloy joints brazed with a low-melting-point 62.7Zr–11.0Ti–13.2Cu–9.8Ni–3.3Be amorphous filler metal. Mater. Charact. **81**, 19–27 (2013). https://doi.org/10.1016/j.matchar.2013.04.002
67. Nimonic 80A http://www.superalloy.com.cn/EN/Alloy/Nimonic80A/. Accessed 26 Jul 2021
68. K. Sairam, J.K. Sonber, T.S.R.C. Murthy, C. Subramanian, R.K. Fotedar, R.C. Hubli, Reaction spark plasma sintering of niobium diboride. Int. J. Refract. Met. Hard Mater. **43**, 259–262 (2014). https://doi.org/10.1016/j.ijrmhm.2013.12.011
69. J. Brenneman, J. Wei, Z. Sun, L. Liu, G. Zou, Y. Zhou, Oxidation behavior of GTD111 Ni-based superalloy at 900 °C in air. Corros. Sci. **100**, 267–274 (2015). https://doi.org/10.1016/j.corsci.2015.07.031
70. B.S. Babu, V. Srikanth, Y. Balram, T. Vishnuvardhan, M.A.A. Baig, Numerical analysis on the indentation behavior of Ti–6Al–4V alloy. Mater. Today Proc. **19**, 827–830 (2019). https://doi.org/10.1016/j.matpr.2019.08.139
71. L. Umamaheswararao, K. Mallikarjunarao, Design and Analysis of turbine blade by using fem. Int. J. Mech. Eng. **4**(1), 1–8 (2015)
72. A. Shaw, Physical properties of various conductive diborides and their binaries. Grad. Theses Diss. (2015). Available: http://lib.dr.iastate.edu/etd/14496
73. D. Demirskyi, I. Solodkyi, T. Nishimura, O.O. Vasylkiv, Fracture and property relationships in the double diboride ceramic composites by spark plasma sintering of TiB_2 and NbB_2. J. Am. Ceram. Soc. **102**(7), 4259–4271 (2019). https://doi.org/10.1111/jace.16276
74. D. Siebörger, H. Knake, U. Glatzel, Temperature dependence of the elastic moduli of the nickel-base superalloy CMSX-4 and its isolated phases. Mater. Sci. Eng. A. **298**(1–2), 26–33 (2001). https://doi.org/10.1016/s0921-5093(00)01318-6
75. M. Papa, R.J. Goldstein, F. Gori, Effects of tip geometry and tip clearance on the mass/heat transfer from a large-scale gas turbine blade. J. Turbomach. **125**(1), 90–96 (2003). https://doi.org/10.1115/1.1529190
76. M. Beghini et al., High temperature fatigue testing of gas turbine blades. Procedia Struct. Integr. **7**, 206–213 (2017). https://doi.org/10.1016/j.prostr.2017.11.079
77. D. Demirskyi, I. Solodkyi, T. Nishimura, Y. Sakka, O. Vasylkiv, High-temperature strength and plastic deformation behavior of niobium diboride consolidated by spark plasma sintering. J. Am. Ceram. Soc. **100**(11), 5295–5305 (2017). https://doi.org/10.1111/jace.15048
78. B. Wilthan, K. Preis, R. Tanzer, W. Schützenhöfer, G. Pottlacher, Thermophysical properties of the Ni-based alloy nimonic 80A up to 2400 K, II. J. Alloy. Compd. **452**(1), 102–104 (2008). https://doi.org/10.1016/j.jallcom.2006.11.214
79. F.G. Keihn, E.J. Keplin, High-Temperature thermal expansion of certain group IV and group V diborides. J. Am. Ceram. Soc. **50**(2), 81–84 (1967). https://doi.org/10.1111/j.1151-2916.1967.tb15044.x
80. G.L. Zhunkovskii, T.M. Evtushok, O.N. Grigor'Ev, V.A. Kotenko, P.V. Mazur, Activated sintering of refractory borides. Powder Metall. Met. Ceram. **50**(3–4), 212–216 (2011). https://doi.org/10.1007/s11106-011-9320-2
81. K.K. Sharma, D. Banerjee, S.N. Tewari, Effect of reverse-aging treatment on the microstructure and mechanical properties of Nimonic alloys. Mater. Sci. Eng. **104**, 131–140 (1988). https://doi.org/10.1016/0025-5416(88)90414-4
82. J.H. Du, X.D. Lu, Q. Deng, J.L. Qu, J.Y. Zhuang, Z.Y. Zhong, High-temperature structure stability and mechanical properties of novel 718 superalloy. Mater. Sci. Eng. A. **452–453**, 584–591 (2007). https://doi.org/10.1016/j.msea.2006.11.039
83. A. Singh, A.K. Pujari, B.V.S.S.S. Prasad, Conjugate heat transfer analysis of a rotor blade with coolant channels. Heat Transf. (2021). https://doi.org/10.1002/htj.22205